ACS OMEGA

Article

Cite This: ACS Omega 2018, 3, 15416−15425

http://pubs.acs.org/journal/acsodf

Molecular Engineering and Structure-Related Properties of Squaraine Dyes Based on the Core and Wings Concept

G. Hanumantha Rao,[†,‡] Prem Jyoti Singh Rana,[†] Ramesh Kumar Chitumalla,[§] Joonkyung Jang,[*,§] and Surya Prakash Singh[*,†,†]

[†]Polymers and Functional Materials Division, CSIR-Indian Institute of Chemical Technology, Uppal Road, Tarnaka, Hyderabad 500007, India

[‡]Academy of Scientific and Innovative Research (AcSIR), CSIR-Human Resource Development Centre, (CSIR-HRDC) Campus, Kamla Nehru Nagar, Ghaziabad, Uttar Pradesh 201002, India

[§]Department of Nanoenergy Engineering, Pusan National University, Busan 46241, Republic of Korea

S *Supporting Information*

ABSTRACT: Three new squaraine-based functional π-conjugated molecules were synthesized considering the core and wings concept. The molecules, **SQ-DICN**, **SQ-DIEt-RH**, and **SQ-DICN-RH**, were end-capped with three different wings, such as malononitrile, 2-(3-hexyl-4-oxothiazolidin-2-ylidene)malononitrile, and 3-ethyl-2-thioxothiazolidin-4-one. Among the three dyes, **SQ-DICN-RH** showed the highest molar extinction coefficient. The photoluminescence of all the dyes showed an opposite trend to that of the absorption maximum. The electrochemical results showed that the lowest unoccupied molecular orbital level of all the dyes ranged from −3.72 to −3.82 eV, whereas the highest occupied molecular orbital ranged from −4.89 to −4.94 eV. Solvatochromism was carried out to observe the effects of the solvent containing the dyes. The electronic structure of the dyes was examined using *ab initio* simulations. The dyes were characterized theoretically, and the red-shifted absorption of **SQ-DICN-RH** was explained and correlated with its biradicaloid character and singlet−triplet energy gap.

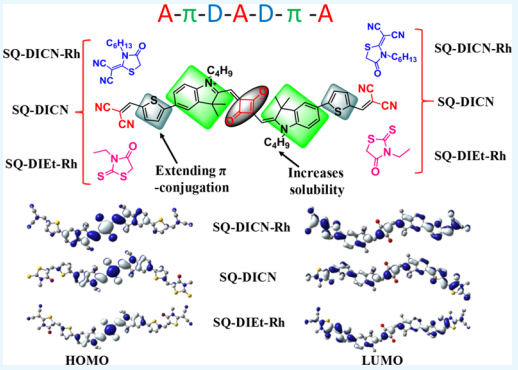

INTRODUCTION

The absorption of photons in the near-infrared (NIR) region by fluorescent dyes has an increasing number of applications in biomedical science,[1] materials science, and nanotechnology.[2] A series of NIR dyes, such as BODIPY, DPP, phthalocyanine, and squaraine, have been reported.[3] Among them, squaraine dyes have shown promising applications in fluorescent probes,[4,5] photosensitizers [in dye-sensitized solar cells (DSSCs)],[6] electron donors [in organic photovoltaic (OPV)],[7] optical storage media,[8−10] sensitizers for photodynamic cancer therapy,[11−13] and two-photon absorbing materials.[14,15] Because OPV devices are being fabricated with a blend of fullerene and polymer/small molecule (SM) derivatives, which play a key role in enhancing the power conversion efficiency (PCE).[16] Fullerene derivatives such as phenyl-C61-butyric acid methyl ester and phenyl-C71-butyric acid methyl ester have been widely accepted as electron-accepting materials, whereas polymers are used as donor materials. Fullerenes have high dominance in OPV because of their advantageous properties such as (i) electron-withdrawing capability, (ii) high electron mobility, and (iii) three-dimensional transportability of electrons due to their shape.[17]

Notwithstanding advantages, fullerene has some limitations, that is, it does not cover the entire visible region of the incident solar spectrum because of weak absorption, cost-effective synthesis, and effects in the aggregation and morphology of thin films. In the past few years, a considerable concentration has been waged on the development of nonfullerene acceptors (NFAs)[18,19] in OPVs instead of fullerene derivatives. Novel NFAs show number of superior properties over the fullerene, such as ease of synthesis, high absorption in the visible to NIR region of the solar spectrum, and structural plasticity, which allows tuning the energy levels of donors and acceptors. By considering all these superior properties, NFAs have been designed and applied in OPVs. In this regard, Beaujuge et al. reported (compound **1**, **2**, and **3** shown in Figure 1) small molecular acceptors having malononitrile as the end group with a PCE of 5.3%.[20] Lim et al. introduced fluorene/carbazole-containing rhodanine-based acceptors (compound **4** and **5** shown in Figure 1) for OPV and resulted in a PCE of 3.08%.[21] Recently, Zhan et al. reported indacenodithiophene as a core and ethyl rhodamine/malononitrile as an end group[22,23](**6a**, **6b**) and achieved a PCE of 5.12 and 4.81%, respectively. Malononitrile end group-based organic molecules have also

Received: July 29, 2018
Accepted: October 31, 2018
Published: November 13, 2018

DOI: 10.1021/acsomega.8b01809
ACS Omega 2018, 3, 15416−15425

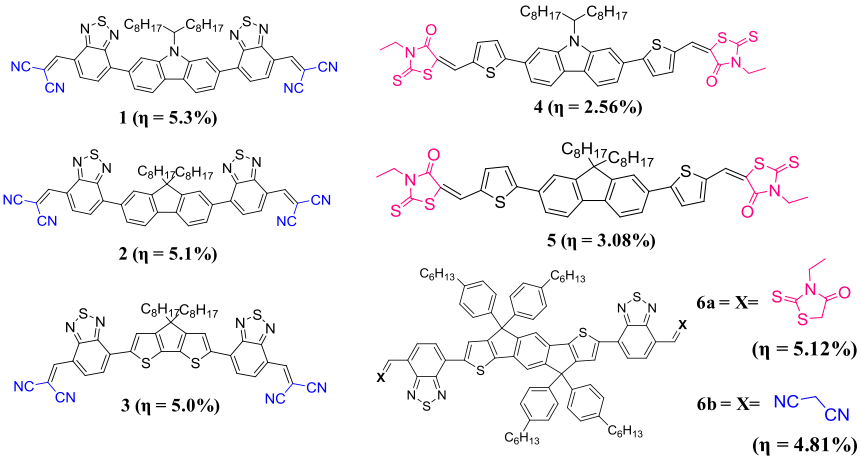

Figure 1. Molecular structures of NFAs based on the core and wings concept.

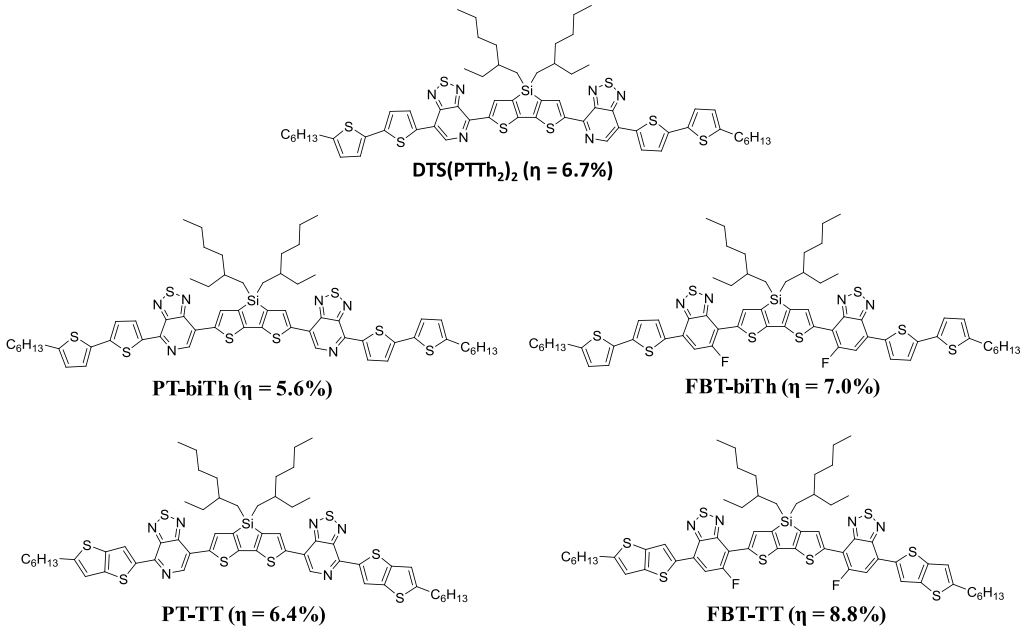

Figure 2. Molecular structures of SMs based on the core and wings concept.

been used in organic field-effect transistors (OFETs) and have achieved the mobility[24,25] up to 0.64 $cm^2 V^{-1} s^{-1}$.

NIR squaraine dyes, showing absorption beyond 700 nm, helped in constructing transparent and semitransparent photovoltaic devices.[26,27] The squaraine dyes were classified into two categories: symmetrical and unsymmetrical. The symmetrical squaraine molecules followed a simple synthetic pathway and could be synthesized *via* the condensation of electron-rich molecules (such as indolium salts) with squaric acid. The electronic and optical properties of such dyes depend on their energy gap, that is, the energy difference between the lowest unoccupied molecular orbital (LUMO) and highest occupied molecular orbital (HOMO). The absorption and emission properties of fluorescent dyes that undergo wide changes in charge dispersal and photoexcitation processes involving intramolecular electron transfer are quite sensitive to the nature of the solvent used.

Because squaraine dyes possess reasonable photo- and thermal stability and exhibit an intense absorption peak, they have been used widely as an electron-donating material in the bulk-heterojunction (BHJ) solar cells.[28−30] Although considerable attention has been paid toward the molecular engineering of new squaraine dyes, there have been few studies on the structural−property relationship of these promising optoelectronic materials.[31] In general, the molecular architecture of these squaraine dyes is in a donor (D)−acceptor (A)−donor fashion. Their photophysical and electrochemical properties can be tuned finely further by altering the basic architecture through the design of a newer concept, that is, donor−π−acceptor−donor (D−π−A−D), donor−π−acceptor−π−donor (D−π−A−π−D), and acceptor−π−donor−acceptor−π−donor (A−π−D−A−π−D). The most successful design of photonic materials was reported by the Bazan research group.[32] They introduced a new class of small molecule donor materials for solution-processed OPVs. Before this work, SMs appeared to be intrinsically inferior to polymers in their ability to generate useful BHJ solar cells. They developed a new framework that can generally be explained as consisting of an electron-rich central core flanked by a poor electron-withdrawing unit and finished with π-conjugated end caps. This scaffold recommended the suitable synthetic entry to a wide class of materials with tailored electronic, optical, and physical properties.

DOI: 10.1021/acsomega.8b01809
ACS Omega 2018, 3, 15416−15425

This paper reports three symmetrical novel SQ dyes with the acceptor−π−donor−acceptor−donor−π−acceptor (A−π−D−A−D−π−A) architecture. The three SQ dyes were decorated with three different acceptors as end groups (wings) [malononitrile, 2-(3-hexyl-4-oxothiazolidin-2-ylidene)-malononitrile, and 3-ethyl-2-thioxothiazolidin-4-one], respectively, and a central squaraine unit as the core. This study examined the photochemical properties in different solvents regarding the solubility and potential applications. The geometries (*cis*- and *trans*-isomers) and biradical character of the dyes were analyzed by density functional theory (DFT). The calculated electrochemical and photophysical properties were compared with the experimental data. The reasons behind the red-shifted absorption for **SQ-DICN-RH** were investigated using theoretical simulations.

RESULTS AND DISCUSSION

The core and wings concept is useful for symmetrical systems when compared with another multichromophoric system for absorption of sunlight in the visible to NIR regions of the solar spectrum. Using the core and wings concept, we can attach different kinds of end groups (wings) to know the electronic properties of respective dyes by keeping the core as constant. Bazan et al. proposed a core and an end-capping group concept in SM BHJ solar cells as donors, and they reported the DTS(PTTh$_2$)$_2$ structure based on a core donor−acceptor framework with end-capping units with a PCE of 6.7%.[32] We recently reported four SMs based on the core and wings concept and dithienosilole (DTS) used as a core for four molecules at the center of the molecule as an electron donor (Figure 2).[33]

Squaraine dyes having a multichromophoric system,[34] explored in OPVs, DSSCs, and OFET; however, the core and end-capped (wing) concept are untouched. In this article, we report that three electron-acceptor units [malononitrile or 3-ethyl rhodanine or 2-(3-hexyl-4-oxothiazolidin-2-ylidene)-malononitrile] are connected in conjugation with the central squaraine core moiety, which as a result enhanced the absorption in the solar spectrum and electron affinities. Complete representation of core and wings is shown in Figure 3.

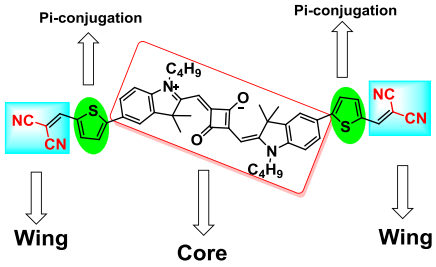

Figure 3. Squaraine structure having the core and wings design.

Absorption and Photoluminescence Spectroscopy. The optical absorption spectra of SQ dyes were collected in dichloromethane (DCM) and are shown in Figure 4; the related data are summarized in Table 1. **SQ-DIEt-RH**, **SQ-DICN**, and **SQ-DICN-RH** dyes show a prominent absorption maximum at 710, 716, and 720 nm with vibration progression at 650, 656, and 661 nm, respectively. The absorption at longer wavelengths was attributed to a charge transfer π−π* transition. The new less-intense broad absorption band in the region from 365 to 450 nm was assigned to the prolonged conjugation occurring from the dicyanovinyl unit. **SQ-DCN-RH**, showing a greater

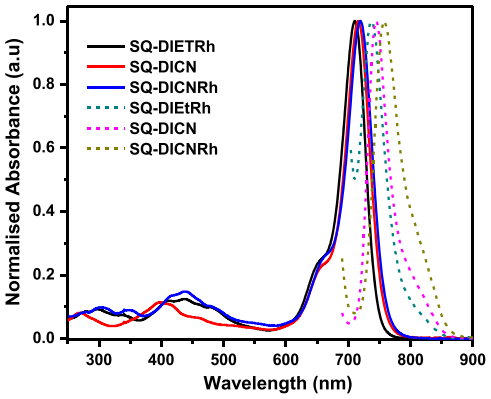

Figure 4. Normalized absorption (solid lines) and photoluminescence (dotted lines) spectra of the SQ dyes in a DCM solution.

Table 1. Absorption and Photoluminescence Data of SQ Dyes in a DCM Solution at Ambient Temperature

sample code	λ_{abs} (nm)[a]	λ_{em} (nm)[b]	ε (dm^3 mol^{-1} cm^{-1}) × 10^5	Stokes shift (nm)[c]
SQ-DIEt-RH	710	738	1.18	28
SQ-DICN	716	745	1.20	29
SQ-DICN-RH	720	757	1.33	27
SQ-2Br	643	653	1.17	10

[a]Optical absorption maxima. [b]Emission maxima of SQ dyes in the DCM solution. [c]Difference of absorption and emission maximum.

λ_{max} with respect to the other two SQ dyes, was attributed to the presence of extended conjugation and the dicyanovinyl unit. The emission spectra of the three SQ dyes were measured in a DCM solution and are displayed in Figure 4. The fluorescence spectrum of **SQ-DIEt-RH**, **SQ-DICN**, and **SQ-DICN-RH** dyes showed the emission maximum at 738, 745, and 757 nm with a Stokes shift of 27, 29, and 28 nm, respectively, which is in contrast to the absorption maxima trend.[35] These smaller Stokes shifts arise because of the conformational rigidity, that is, the presence of an analogous configuration of the dye molecules in the ground state as well as in the excited states.

Electrochemical Properties. The redox propensity of the dyes was analyzed by cyclic voltammetry (CV) and differential pulse voltammetry in DCM solution shown in Figure 5. Table 2 lists the relevant data of the dyes. All dyes showed two quasi-reversible oxidation couples attributed to simultaneous electron elimination from indolium salts. For the first anodic peak, **SQ-DCN** showed difficult oxidation because of the strong electron-withdrawing nature of the dicyanovinyl unit on both sides of the squaraine building block. The order of the oxidation pattern is as follows: **SQ-DIEt-RH** = **SQ-DCN-RH** (0.53) < **SQ-DCN** (0.57). On the other hand, the second oxidation was similar for all dyes due to the same electron richness of the cation dyes. Therefore, the band gap of **SQ-DCN** is lower than that of the other dyes. The HOMO of the dyes was calculated from the oxidation of SQ dyes with respect to the ferrocene/ferrocenium cation. The HOMO and LUMO of **SQ-DCN** were high compared to the other dyes and it can act as a better donor to construct the organic solar cell devices by blending the PCBM electron acceptor. The remaining rhodanine and dicyanorhodanine dyes showed similar HOMO and LUMO values.

Solvatochromism. To examine excited-state properties of SQ dyes, the absorption and the emission profile of all the SQ dyes were scrutinized with different solvents, that is, toluene

DOI: 10.1021/acsomega.8b01809
ACS Omega 2018, 3, 15416−15425

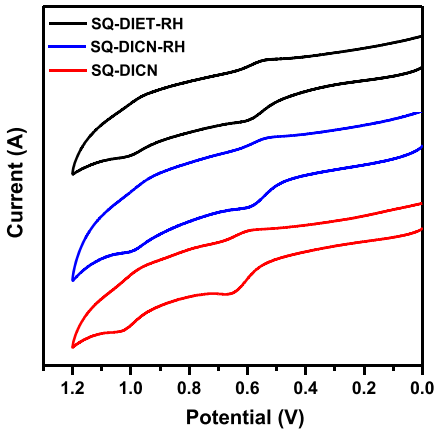

Figure 5. Cyclic voltammograms of the squaraine dyes [1 mM solution of SQ dyes in DCM using 0.1 M of the supporting electrolyte $(Bu)_4NPF_6$, reference electrode (Ag/AgCl), and internal standard ($[Fc]^+/[Fc]^0$) with a scan rate of 100 mV s^{-1}].

(TOL), chloroform (CHL), DCM, tetrahydrofuran (THF), ethyl acetate (EA), and dimethylformamide (DMF) as shown in Figure 6. Generally, all the absorption profiles of the SQ dyes are insensitive to the solvent polarity, which indicates the presence of the less polar ground state. The absorption spectra of **SQ-DICN-RH**, **SQ-DICN**, and **SQ-DIEt-RH** in different solvents did not show a significant shift in the λ_{max} value, that is, 10, 4, and 13 nm, respectively, in the ground state. On the other hand, in emission spectra, **SQ-DICN-RH** showed an increase in wavelength from 738 nm (nonpolar solvent) to 761 nm (polar solvent); **SQ-DICN** emission spectra showed an increase in wavelength from 744 to 768 nm, and similarly, the **SQ-DIEt-RH** emission spectra ranged from 736 to 760 nm. In **SQ-DICN-RH**, 740 nm emissions were observed in DCM and were red-shifted 20 nm in DMF because of the increase in polarity.

In contrast, the dye **SQ-DICN** in DCM showed an emission maximum at 745 nm, whereas it was 760 nm in DMF. **SQ-DIET-RH** in EA showed an emission at 730 nm, showing a 30 nm shift compared to that in DMF. Therefore, the emission spectra showed a reasonable positive response toward the solvatochromism with increasing solvent polarity. This suggests that the excited state of all the SQ dyes is more polar than the ground state because they may have a planar type structure in the excited state. In general, the difference in the Stokes shift between the polar and nonpolar solvents is due to charge transfer from the organic luminogens in the excited state.[36]

Spectroelectrochemical Properties. The spectroelectrochemistry study was carried out to better understand the spectroscopic and electrochemical behavior of the dyes. This study focused mainly on the UV−visible region because electron transfer in the electrochemical system occurs in the same region because of the high molar absorption coefficient of the dyes. CV of all three dyes was performed in DCM and showed two quasi-reversible oxidation waves in the range from 0.53 to 0.57 and 0.94 to 0.96 V in the anodic region versus calomel electrode. Upon applying the controlled oxidation potential to all the SQ dyes, the intense absorption peak in the visible region decreased gradually with the formation of isosbestic points nearly at 582 and 757 nm, which indicates the oxidation outcome in a single product. This might be due to the squaraine cation radical formation. The potential of 0.94−0.96 V was also applied for all the dyes, but no significant change in the absorption spectra was observed. **SQ-DICN-RH** shows a fast gradual decrease because of the presence of an electron acceptor and extended conjugation. When applied oxidation potential was removed, the absorption spectra returned almost to its original absorption. Figure 7 presents the UV−visible spectroelectrochemical changes with the **SQ-DICN-RH**, **SQ-DICN**, and **SQ-DIEt-RH** dyes recorded in DCM at the respective applied potentials.

Theoretical Calculations. To gain deeper insights into the structural (geometrical isomerism), electrochemical, and optical behavior (bathochromic shift for **SQ-DICN-RH**), a detailed theoretical investigation was carried out using first-principles *ab initio* simulations. The *cis*- and *trans*-isomers of the synthesized SQ dyes were modeled; Figure 8 shows the optimized geometries and the deviations in the dihedral angles of their wings. The corresponding geometries of the *cis*-isomers are given in Figure S18 in the Supporting Information. The *trans*-isomer of the SQ dye is relatively more stable than the corresponding *cis*-isomer and the relative energies are given in Figure S18. The *trans*-isomers of **SQ-DICN**, **SQ-DIEt-RH**, and **SQ-DICN-RH** were 0.95, 0.93, and 0.96 kcal/mol more stable, respectively, than the corresponding *cis*-isomers. The low stability of the cis-isomers can be attributed to the steric hindrance caused by the one-sided alignment of the wings with respect to the squaraine moiety. The ground-state geometries of the *cis*-isomers possess higher dipole moments than the corresponding *trans*-isomers. Both the *cis*- and *trans*-isomers were planar and differed only in the orientation of the wings attached to the squaraine moiety.

The frontier molecular orbitals (FMOs) of each dye were calculated at the B3LYP/6-31G(d) level of theory. The electron cloud distribution in the FMOs of the dyes is shown in Figure 9, whereas Figure S19 in the Supporting Information shows the corresponding electron density distribution of *cis*-isomers. For both the *cis*- and *trans*-isomers, the electron density was localized mainly over the squaraine core in the HOMO and was dispersed toward the attached wings in the LUMO. The calculated HOMOs and LUMOs of the dyes were well matched with those obtained from the CV measurements. The theoretical HOMO eigenvalues of the dyes were −5.92, −5.82, and −5.86 eV, respectively, for **SQ-DICN**, **SQ-DIEt-RH**, and **SQ-DICN-RH**.

Table 2. Electrochemical Data of SQ Dyes in DCM under an Inert Condition at RT[a]

sample code	E^1_{ox}	E^2_{ox}	E^*_{ox}	E_{0-0} (eV)	HOMO (eV)	LUMO (eV)	ΔG_{inj} (V)
SQ-DCN-Et-RH	0.532	0.94	1.15	1.68	−4.89	−3.72	0.66
SQ-DCN	0.576	0.96	1.12	1.69	−4.94	−3.82	0.62
SQ-DCN-RH	0.531	0.95	1.16	1.69	−4.89	−3.72	0.65
SQ-2Br	0.651	1.11	1.24	1.90	−4.99	−3.09	

[a] E^*_{ox} (excited-state oxidation potential) of the SQ dyes was evaluated by the ground-state potential of the SQ dye in the Rehm−Weller equation ($E^*_{ox} = E_{ox} - E_{0-0}$). E_{ox} was calculated from CV; it is the ground-state oxidation potential. The thermodynamic driving force of the electron injection is as follows: $(\Delta G_{inj}) = E^*_{ox} - E_{CB}$.

DOI: 10.1021/acsomega.8b01809
ACS Omega 2018, 3, 15416−15425

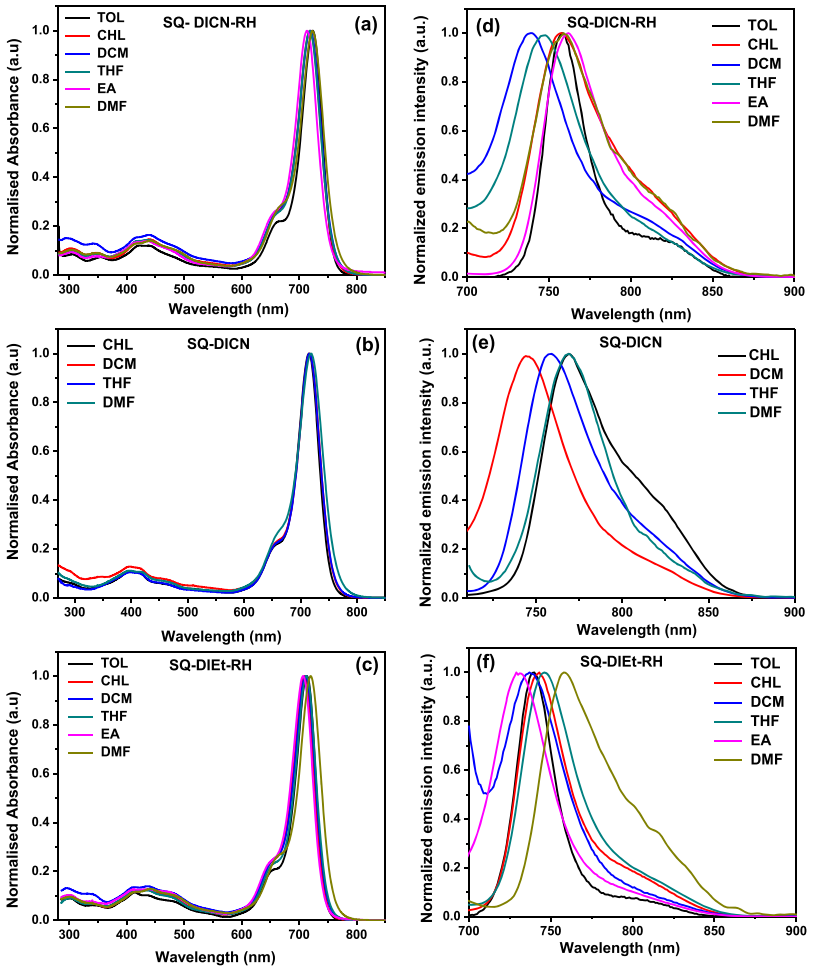

Figure 6. Absorption (a–c) and emission (d–f) spectra of the SQ dyes in different solvents.

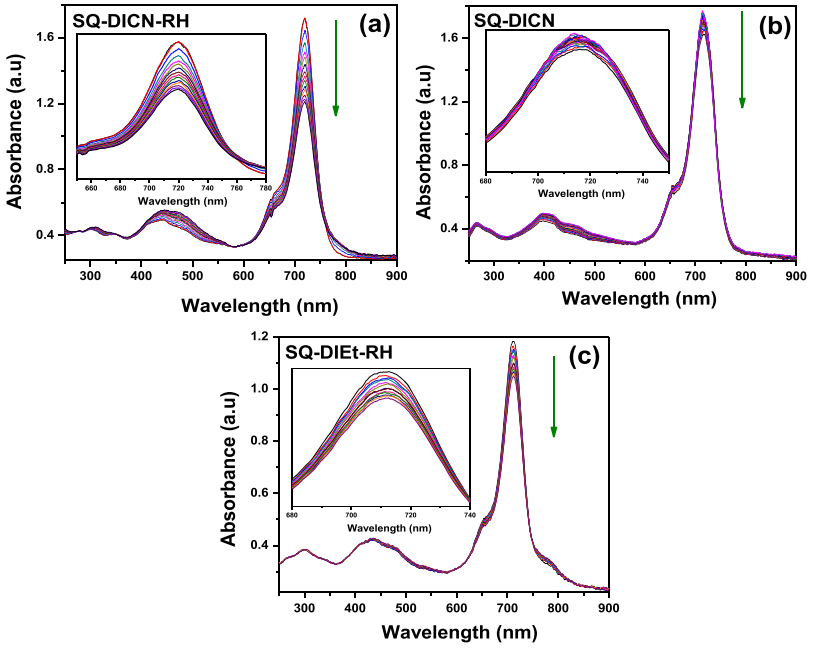

Figure 7. Absorption spectroelectrochemical changes of (a) **SQ-DICN-RH**, (b) **SQ-DICN**, and (c) **SQ-DIEt-RH** dyes recorded in DCM at the respective applied potentials.

The LUMO energies were calculated by adding the time-dependent DFT (TDDFT) transition energy ($E_{S_0 \rightarrow S_1}$) to the corresponding HOMO energy, rather than considering the unreliable Kohn–Sham LUMO eigenvalue.[37] The LUMO

DOI: 10.1021/acsomega.8b01809
ACS Omega 2018, 3, 15416–15425

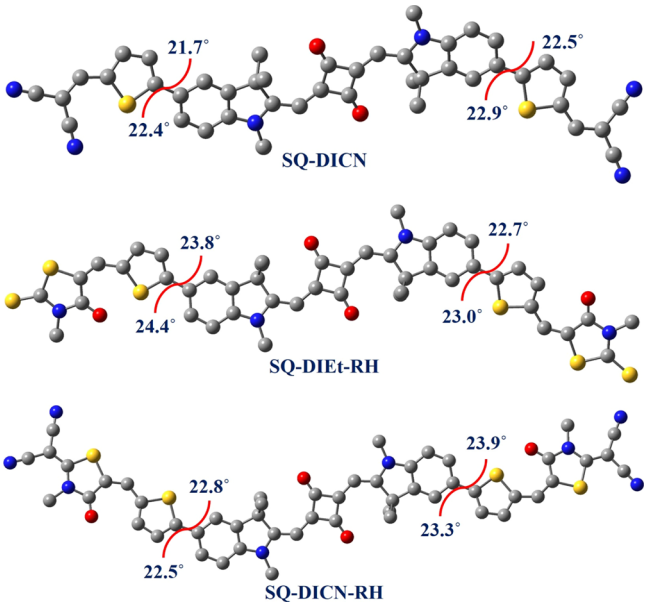

Figure 8. Ground-state optimized structures of the SQ dyes (*trans*-isomers) and the deviations from the planarity of their wings. Hydrogen atoms were omitted for clarity.

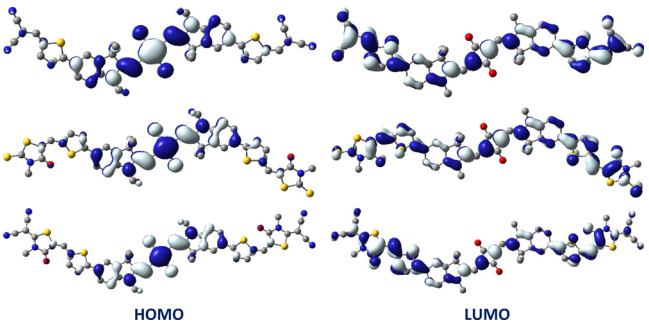

Figure 9. Isodensity plots (isosurface = 0.02 e Å^{-3}) of the FMOs of **SQ-DICN** (top), **SQ-DIEt-RH** (middle), and **SQ-DICN-RH** (bottom).

energies for **SQ-DICN**, **SQ-DIEt-RH**, and **SQ-DICN-RH** obtained from this method were −4.26, −4.12, and −4.21 eV, respectively. The calculated LUMO eigenvalues were in good agreement with those obtained experimentally.

The optical properties of the dyes were evaluated using the TDDFT formalism; Figure 10 shows the simulated UV−visible absorption spectra. The simulated absorption spectra reproduced the main bands observed in the experimental spectra. The calculated absorption maxima (λ_{max}) for **SQ-DICN**, **SQ-DIEt-RH**, and **SQ-DICN-RH** in the low energy region were 748, 728, and 752 nm, respectively. These intense transitions were attributed mainly to HOMO → LUMO excitation. The other two absorption peaks with less intensity were observed at *ca.* 550 nm and *ca.* 450 nm. The red-shifted absorption (NIR absorption) of the squaraine dyes can be attributed to their biradicaloid character (BRC) rather than the charge transfer.[38,39] The method suggested by Nakano et al. based on orbital occupation numbers was used to estimate the BRC percentage of the three dyes.[40]

$$\mathrm{BRC} = \left(1 - \frac{2S_i}{1 + S_i^2}\right) \times 100$$

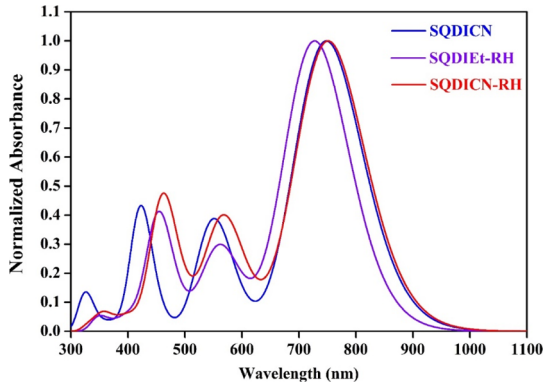

Figure 10. Simulated UV−visible absorption spectra of the SQ dyes obtained at the TD-B3LYP/6-31G(d) level of theory in a CHL solution.

where $S_i \left(= \frac{n_{\mathrm{HOMO}-i} - n_{\mathrm{LUMO}+i}}{2} \right)$ is the orbital overlap.

The calculated BRC percentage of the dyes was 12.9 and 13.3% for **SQ-DICN** and **SQ-DICN-RH**, respectively, whereas the **SQ-DIEt-RH** dye did not show any BRC. The red-shifted absorption (λ_{cal} = 752 nm) of **SQ-DICN-RH** can be attributed to the high BRC (13.3%) among the three dyes. Although the calculated BRC of the dyes was low, the order of the BRC is in accordance with that of the absorption maxima of the dyes. As per the earlier reports, the BRC is underestimated by DFT functionals;[41,42] hence, we used the UHF/6-31G(d) level of theory to evaluate the BRC of the dyes. The adiabatic singlet−triplet energy gap (ΔE_{S-T}) was taken as the difference in the energies of the lowest singlet ground state (S_0) and the corresponding lowest triplet state (T_1). The S_0 geometries were considered to be the initial geometries to optimize T_1 at the UB3LYP/6-31g(d) level of theory. The calculated ΔE_{S-T} of the dyes was 21.51, 21.68, and 21.41 kcal/mol for **SQ-DICN**, **SQ-DIEt-RH**, and **SQ-DICN-RH**, respectively. The relatively high ΔE_{S-T} values exhibited by the dyes are responsible for their lower BRC (Table 3).

CONCLUSIONS

Three new squaraine dyes were synthesized and characterized systematically. The core and wings concept was adopted to design these dyes, which is the most successful design for developing high-performing photonic materials. The absorption and emission spectra of these squaraine dyes were recorded in DCM (10^{-5} M). Among these three dyes, **SQ-DICN-RH** showed a greater λ_{max} with respect to the other two SQ dyes because of the presence of extended conjugation and a dicyanovinyl unit. The absorption spectra of these dyes were not sensitive toward the solvent polarity, which indicates the less polar ground state but the emission spectra showed a reasonable positive response toward the solvatochromism with increasing solvent polarity. This suggests that the excited state of all the SQ dyes is more polar than the ground state. The results agreed well with the computational study. This study paves the way to the design and synthesis of other derivatives for high-performing optoelectronic materials.

EXPERIMENTAL SECTION

General Methods and Materials. All precursor materials, 5-formyl-2-thienylboronic acid, malononitrile, 3-ethyl rhodamine, and squaric acid, were purchased directly from

DOI: 10.1021/acsomega.8b01809
ACS Omega 2018, 3, 15416−15425

Table 3. Simulated Electrochemical and Optical Properties of the Dyes Collected at the B3LYP/6-31G(d) Level of Theory

dye	HOMO (eV)	$E_{S_0 \rightarrow S_1}$[a] (eV)	LUMO[b] (eV)	λ_{cal} (nm)	f[c]	μ_{ge}[d] (D)	predominant contribution	BRC (%)	ΔE_{S-T}[e]
SQ-DICN	−5.92	1.66	−4.26	748	2.0980	7.19	H → L (99%)	12.9	21.51
				551	0.8164	3.85	H → L + 2 (93%)		
				423	0.8621	3.46	H − 3 → L (54%)		
SQ-DIEt-RH	−5.82	1.70	−4.12	728	2.4760	7.70	H → L (98%)	0	21.68
				562	0.7298	3.67	H → L + 2 (92%)		
				455	0.8288	3.52	H − 1 → L + 1 (85%)		
SQ-DICN-RH	−5.86	1.65	−4.21	752	2.3913	7.69	H → L (98%)	13.3	21.41
				568	0.9545	4.23	H → L + 2 (91%)		
				462	0.9620	3.83	H − 1 → L + 1 (77%)		

[a]TDDFT transition energy ($S_0 \rightarrow S_1$). [b]LUMO = HOMO + E_{0-0}. [c]Oscillator strength. [d]Ground- to excited-state transition dipole moment. [e]ΔE_{S-T} in kcal/mol.

Scheme 1. Synthetic Procedure of the Novel SQ Dyes

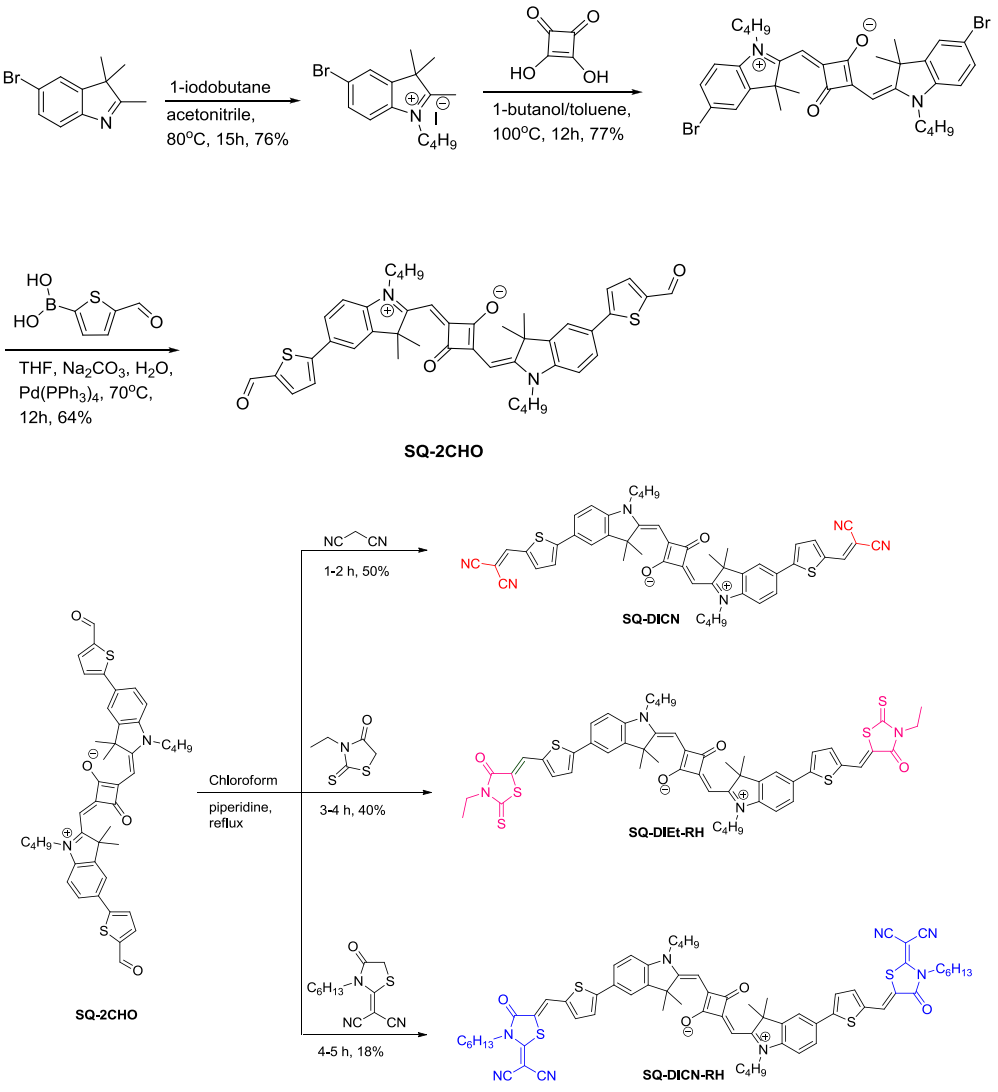

commercial sources and used as received. The ^{1}H and ^{13}C NMR spectra were measured using AVANCE ACP-300, AVANCE-400, and AMX2-500 spectrometers at 300, 400, and 500 MHz, respectively, using tetramethylsilane (TMS) as an internal standard. High resolution mass spectrometry (HRMS) and matrix-assisted laser desorption/ionization time of flight (MALDI-TOF) were performed on a Shimadzu LCMS-2010 EV model with an ESI probe. CV was performed on CH Instruments with a three-electrode system consisting of a glassy carbon working electrode, an Ag/AgCl reference electrode, and a platinum wire counter electrode. A UV−visible spectrophotometer was used to record the absorption spectra of the SQ dyes in DCM solution. The redox potentials of the dyes were measured in DCM containing 0.1 M Bu_4NClO_4 at a scan rate of 100 mV s^{-1}.

DOI: 10.1021/acsomega.8b01809
ACS Omega 2018, 3, 15416−15425

Synthesis. Scheme 1 presents the synthetic pathway used to prepare the dyes, **SQ-DICN**, **SQ-DIEt-RH**, and **SQ-DICN-RH**. 5-Bromo-2,3,3-trimethyl-3*H*-indole and[43] 2-(3-hexyl-4-oxothiazolidin-2-ylidene)malononitrile[44] were synthesized using the methodologies reported in the literature.[43,44] The designed intermediate symmetrical squaraine dye, **SQ-2CHO**, was synthesized *via* Suzuki cross-coupling between **SQ-2Br** and 5-formyl-2-thienylboronic acid. A condensation reaction between **SQ-2CHO** and the end groups, malononitrile, 3-ethyl rhodamine, and 2-(3-hexyl-4-oxothiazolidin-2-ylidene)-malononitrile, in CHL with base afforded the target molecules. All compounds were characterized thoroughly by nuclear magnetic resonance (NMR, ^{1}H and ^{13}C) spectroscopy, Fourier transform infrared spectroscopy, MALDI, and HRMS.

5-Bromo-1-butyl-2,3,3-trimethyl-3H-indol-1-ium Iodide. 5-Bromo-2,3,3-trimethyl-3*H*-indole (2 g, 8.4 mmol), iodobutane (3.09 g, 16.8 mmol), and acetonitrile (15 mL) were taken in a round bottom flask. The reaction mixture was heated under reflux up to 12 h. The solvent was removed using vacuum and washed with diethyl ether and *n*-pentane several times to obtain compound (**2**) as a brown color solid. Yield: 1.8 g (76%). mp 162−164 °C. ^{1}H NMR (400 MHz, $CDCl_3$, TMS): δ (ppm) 7.70−7.74 (m, 2H), 7.61 (d, J = 8 Hz, 1H), 4.67 (t, J = 8 Hz, 2H), 3.08 (s, 3H), 1.88−1.96 (m, 2H), 1.68 (s, 6H), 1.47−1.55 (m, 2H), 1.02 (t, J = 8 Hz, 3H). ^{13}C NMR (100 MHz, $CDCl_3$): δ (ppm) 195.5, 143.3, 139.8, 132.8, 126.8, 124.7, 117.1, 54.8, 50.3, 29.9, 23.2, 20.2, 17.0, 13.7 ppm.

*(Z)-4-((5-Bromo-1-butyl-2,3,3-trimethyl-3H-indol-1-ium-2-yl)methylene)-2-((E)-(5-bromo-1-butyl-3,3-dimethylindolin-2-ylidene)methyl)-3-oxocyclobut-1-enolate (**SQ-2Br**).* Squaric acid (0.25 g, 2.19 mmol) and 5-bromo-1-butyl-2,3,3-trimethyl-3*H*-indol-1-ium iodide (1.29 g, 4.38 mmol) were dissolved in a mixture of 10 mL TOL/*n*-butanol (1:1 v/v, 25 mL) in a two-necked round bottom flask, which was followed by the addition of one drop of pyridine. The reaction mixture was refluxed for 12 h using a Dean−Stark apparatus. After cooling the reaction mixture, the solvents were removed using vacuum. To the crude product, DCM was added and washed with water, dried over Na_2SO_4, and purified by column chromatography on silica gel using DCM/methanol (97:3, v/v) as the eluent to obtain **SQ-2Br**. mp 258−260 °C, blue solid. Yield: 1.12 g (77%). IR (KBr) $\tilde{\nu}$: 3446, 2926, 1610 ($\nu_{C=O}$) cm^{-1}. ^{1}H NMR (400 MHz, $CDCl_3$, TMS): δ (ppm) 7.44−7.45 (m, 2H), 7.424−7.429 (m, 1H), 7.404−7.408 (m, 1H), 6.85 (s, 1H), 6.83 (s, 1H), 5.95 (s, 2H), 3.95 (br s, 4H), 1.78 (s, 16H), 1.42−1.47 (m, 4H), 0.98 (t, J = 8 Hz, 6H). ^{13}C NMR (100 MHz, $CDCl_3$): δ (ppm) 182.0, 180.2, 169.3, 144.1, 141.4, 130.5, 125.6, 116.4, 110.6, 87.0, 49.2, 43.5, 28.9, 26.9, 20.2, 13.7.

*(Z)-4-((1-Butyl-5-(5-formylthiphen-2-yl)-3,3-dimethyl-3H-indol-1-ium-2-yl)methylene)-2-((E)-(1-butyl-5-(5-formylthiphen-2-yl)-3,3-dimethylindolin-2-ylidene)methyl)-3-oxocyclobut-1-enolate (**SQ-2CHO**).* **SQ-2Br** (0.1 g, 0.15 mmol) and 5-formyl-2-thienylboronic acid (0.07 g, 0.4 mmol) were dissolved in a round bottom flask containing 10 mL of dry THF in a nitrogen atmosphere. Subsequently, 1 mL of 2 M Na_2CO_3 solution and $Pd(PPh_3)_4$ (0.05 equiv) were added. The reaction mixture was degassed with nitrogen for approximately 15 min and refluxed for 18 h under nitrogen conditions. After cooling the reaction mixture, the solvent was removed using vacuum. DCM was then added and the mixture was washed twice with water, dried over Na_2SO_4, and purified by column chromatography using DCM/methanol (95:5, v/v) to obtain **SQ-2CHO**. mp 242−244 °C, green solid. Yield: 70 mg (64%). IR (KBr) $\tilde{\nu}$: 3421, 2925, 1658 ($\nu_{C=O}$), 1597 ($\nu_{C=O}$) cm^{-1}. ^{1}H NMR (500 MHz, $CDCl_3$, TMS): δ (ppm) 9.88 (s, 2H), 7.74 (d, J = 5 Hz, 2H), 7.44−7.48 (m, 4H), 7.40 (d, J = 5 Hz, 2H), 7.03 (d, J = 10 Hz, 2H), 6.04 (s, 2H), 4.02 (br s, 4H), 1.84 (s, 12H), 1.45−1.53 (m, 4H), 1.24−1.34 (m, 4H), 1.01 (t, J = 10 Hz, 6H). ^{13}C NMR (100 MHz, $CDCl_3$): δ (ppm) 182.5, 180.3, 169.6, 153.8, 143.4, 141.9, 137.5, 132.0, 131.9, 128.8, 128.5, 128.3, 126.5, 123.6, 120.2, 109.9, 87.7, 76.9, 49.1, 43.7, 29.1, 27.1, 20.3, 13.8.

General Synthetic Procedure for SQ-DICN, SQ-DIEt-RH, and SQ-DICN-RH. In a two-necked round bottom flask, the corresponding **SQ-2CHO** and malononitrile or 3-ethyl rhodanine or 2-(3-hexyl-4-oxothiazolidin-2-ylidene)-malononitrile were placed in 6 ml of dry $CHCl_3$. To this, one drop of piperidine was added and the resulting mixture was refluxed. The reaction mixture was observed by TLC. Upon completion of the reaction, it was allowed to cool to room temperature followed by work-up with water, drying over Na_2SO_4, and concentration under vacuum. The final product was separated by the column chromatography technique and DCM/methanol (99:1, v/v) as the eluent to obtain the pure compounds.

*(Z)-4-((1-Butyl-5-(5-(2,2-dicyanovinyl)thiophen-2-yl)-3,3-dimethyl-3H-indol-1-ium-2-yl)methylene)-2-((E)-(1-butyl-5-(5-(2,2-dicyanovinyl)thiophen-2-yl))-3,3-dimethylindolin-2-ylidene)methyl)-3-oxocyclobut-1-enolate (**SQ-DICN**).* **SQ-2CHO** (50 mg, 0.06 mmol) and malononitrile (13 mg, 0.20 mmol) were used to obtain **SQ-DICN**. Yield: 28 mg, (50%) was obtained as a solid. mp 277−279 °C. IR (KBr) $\tilde{\nu}$: 3448, 2926, 2217 ($\nu_{C\equiv N}$), 1593 ($\nu_{C=O}$) cm^{-1}. ^{1}H NMR (500 MHz, $CDCl_3$): δ (ppm) 7.79 (s, 2H), 7.71 (d, J = 5 Hz, 2H), 7.67 (dd, J_1 = 5 Hz, J_2 = 1.15 Hz, 2H), 7.61 (d, J = 5 Hz, 2H), 7.44 (d, J = 5 Hz, 2H), 7.04 (d, J = 10 Hz, 2H), 6.08 (s, 2H), 4.03 (br s, 4H), 1.84 (s, 12H), 1.81−1.84 (m, 4H), 1.61 (s, moisture), 1.44−1.52 (m, 4H), 1.01 (t, J = 10 Hz, 6H). ^{13}C NMR (100 MHz, $CDCl_3$): δ (ppm) 159.5, 159.0, 158.6, 158.2, 150.5, 143.9, 140.3, 127.3, 116.0, 113.1, 111.1, 110.3, 49.7, 44.2, 33.2, 29.6, 29.3, 26.7, 26.6, 20.1, 13.7. ESI m/z calcd for $[M]^+$ ($C_{50}H_{44}N_6O_2S_2$), 825.05; found, 825.

*(Z)-4-((1-Butyl-5-(5-((Z)-(3-ethyl-4-oxo-2-thioxothiazolidin-5-ylidene)methyl)thiophen-2-yl)-3,3-dimethyl-3H-indol-1-ium-2-yl)methylene)-2-((E)-(1-butyl-5-(5-(-((Z)-(3-ethyl-4-oxo-2-thioxothiazolidin-5-ylidene)methyl)thiophen-2-yl)-3,3-dimethylindolin-2-ylidene)methyl)-3-oxocyclobut-1-enolate (**SQ-DIEt-RH**).* **SQ-2CHO** (50 mg, 0.06 mmol) and 3-ethyl rhodanine (22 mg, 0.13 mmol) were used to produce **SQ-DIEt-RH**. Yield: 28 mg, (40%) was obtained as solid. mp 280−282 °C. IR (KBr) $\tilde{\nu}$: 3418, 2925, 1699 ($\nu_{C=O}$), 1581 ($\nu_{C=O}$) cm^{-1}. ^{1}H NMR (500 MHz, $CDCl_3$): δ (ppm) 7.87 (s, 2H), 7.61−7.63 (m, 2H), 7.58−7.59 (m, 2H), 7.38−7.41 (m, 4H), 7.02 (d, J = 8 Hz, 2H), 6.05 (s, 2H), 4.21 (q, 4H), 4.03 (br s, 4H), 1.79−1.84 (m, 14H), 1.60 (s, moisture), 1.46−1.53 (m, 6H), 1.30 (t, J = 8 Hz, 6H), 1.01 (t, J = 8 Hz, 6H). ^{13}C NMR (100 MHz, $CDCl_3$): δ (ppm) 159.6, 159.2, 158.8, 158.4, 116.0, 113.1, 40.0, 38.8, 33.2, 29.6, 29.5, 30.1, 26.7, 22.6, 20.1, 14.1, 13.7, 12.2. MALDI-TOF (ESI, m/z) calcd for $[M]^+$ ($C_{54}H_{54}N_4O_4S_6$), 1015.42; found, 1018.55.

*(Z)-4-((1-Butyl-5-(5-((Z)-(2-(dicyanomethylene)-3-hexyl-4-oxothiazolidin-5-ylidene)methyl)thiophen-2-yl)-3,3-dimethyl-3H-indol-1-ium-2-yl)methylene)-2-((E)-(1-butyl-5-(5-(-((Z)-(2-(dicyanomethylene)-3-hexyl-4-oxothiazolidin-5-ylidene)-methyl)thiophen-2-yl)-)-3,3-dimethylindolin-2-ylidene)-methyl)-3-oxocyclobut-1-enolate (**SQ-DICN-RH**).* **SQ-2CHO**

DOI: 10.1021/acsomega.8b01809
ACS Omega 2018, 3, 15416−15425

(50 mg, 0.06 mmol) and 2-(3-hexyl-4-oxothiazolidin-2-ylidene)malononitrile (34 mg, 0.13 mmol) were used to synthesize **SQ-DICN-RH**. Yield: 15 mg, (18%) was obtained as solid. mp 282−284 °C. IR (KBr) $\tilde{\nu}$: 2926, 2213 ($\nu_{C\equiv N}$), 1719 ($\nu_{C=O}$), 1611 ($\nu_{C=O}$), cm^{-1}. ^1H NMR (400 MHz, $CDCl_3$): δ (ppm)8.07 (s, 2H), 7.67 (d, J = 4 Hz, 1H), 7.65 (d, J = 4 Hz, 1H), 7.61 (m, 2H), 7.48 (d, J = 4 Hz, 2H), 7.43 (d, J = 4 Hz, 2H), 7.05 (s, 1H), 7.03 (s, 1H), 6.05 (s, 2H), 4.22 (t, J = 8 Hz, 4H), 4.04 (br s, 4H), 1.86 (s, 12H), 1.71−1.83 (m, 8H), 1.6 (s, moisture), 1.40−1.52 (m, 9H), 1.33−1.36 (m, 7H), 1.01 (t, J = 8 Hz, 6H), 0.95 (t, J = 8 Hz, 6H). ^{13}C NMR (100 MHz, $CDCl_3$): δ (ppm) 169.5, 166.0, 165.5, 153.3, 143.6, 136.8, 135.5, 128.8, 128.4, 126.7, 124.6, 119.9, 113.3, 112.2, 110.0, 88.0, 55.7, 49.2, 45.3, 43.7, 31.2, 29.1, 28.7, 27.2, 25.6, 22.4, 20.3, 13.9, 13.8. MALDI-TOF (ESI, m/z) calcd for $[M]^+$ ($C_{68}H_{70}N_8O_4S_4$), 1191.59; found, 1191.54.

Computational Details. The Gaussian 09 quantum chemical program was used for DFT and TDDFT calculations of the three SQ dyes.[45] The DFT method was used to examine the structural and electrochemical properties, and the TDDFT method was used for the excited-state properties. Each of the three SQ dyes was modeled with two isomers, that is, *cis* and *trans*. The geometries were optimized with RB3LYP hybrid exchange−correlation functional in combination with the 6-31G(d) basis set.[46] The method employed in the present study has been successfully used to deal with the other biradical systems such as croconate dyes.[47,48] The optimized geometries of the dyes were subjected to vibrational frequency analysis to ensure the real minima on the potential energy surface. All positive harmonic vibrational frequencies confirmed the real minima. Based on the ground state optimized geometries, TDDFT simulations were performed to evaluate the excitation energies and corresponding oscillator strengths. The TDDFT simulations were also performed at the same level of theory, and the solvent effect was included, as used in the experiment. The experimental CHL solution was mimicked using a polarizable continuum model, as implemented in Gaussian 09.[49,50] The excitation energies and oscillator strengths for the first 25 singlet−singlet excitations were evaluated under the TDDFT framework. The input files were prepared, and the results were visualized using the GaussView graphical interface.[51]

■ ASSOCIATED CONTENT

Supporting Information

The Supporting Information is available free of charge on the ACS Publications website at DOI: 10.1021/acsomega.8b01809.

Structural characterization by ^1H, ^{13}C NMR, ESI MS spectra, MALDI-TOF MS spectra, and DFT calculations (PDF)

■ AUTHOR INFORMATION

Corresponding Authors

*E-mail: jkjang@pusan.ac.kr. Phone: +8251-510-7348 (J.J.).

*E-mail: spsingh@iict.res.in. Phone: +9140-2719-1700 (S.P.S).

ORCID

Prem Jyoti Singh Rana: 0000-0003-4819-947X

Ramesh Kumar Chitumalla: 0000-0002-9523-7056

Joonkyung Jang: 0000-0001-9028-0605

Surya Prakash Singh: 0000-0001-5670-7329

Notes

The authors declare no competing financial interest.

■ ACKNOWLEDGMENTS

G.H.R. wishes to thank the AcSIR for PhD enrolment and CSIR for the Senior Research Fellowship. S.P.S. thanks the DST Indo-Poland project DST/INT/POL/P-26/2016. This work was supported by the Korea Research Fellowship Program through the National Research Foundation of Korea (NRF) funded by the Ministry of Science and ICT (2016H1D3A1936765).

■ REFERENCES

(1) Berezin, M. Y.; Zhan, C.; Lee, H.; Joo, C.; Akers, W. J.; Yazdanfar, S.; Achilefu, S. Two-Photon Optical Properties of Near-Infrared Dyes at 1.55 μm Excitation. *J. Phys. Chem. B* **2011**, *115*, 11530−11535.

(2) Qian, G.; Wang, Z. Y. Near-Infrared Organic Compounds and Emerging Applications. *Chem.—Asian J.* **2010**, *5*, 1006−1029.

(3) Singh, S. P.; Sharma, G. D. Near Infrared Organic Semiconducting Materials for Bulk Heterojunction and Dye-Sensitized Solar Cells. *Chem. Rec.* **2014**, *14*, 419−481.

(4) Lee, S.; Rao, B. A.; Son, Y.-A. A highly selective fluorescent chemosensor for Hg^{2+} based on a squaraine-bis(rhodamine-B) derivative: Part II. *Sens. Actuators, B* **2015**, *210*, 519−532.

(5) Ajayaghosh, A. Chemistry of Squaraine-Derived Materials: Near-IR Dyes, Low Band Gap Systems, and Cation Sensors. *Acc. Chem. Res.* **2005**, *38*, 449−459.

(6) Rao, G. H.; Venkateswararao, A.; Giribabu, L.; Singh, S. P. Near-infrared unsymmetrical blue and green squaraine sensitizers. *Photochem. Photobiol. Sci.* **2016**, *15*, 287−296.

(7) Chen, G.; Sasabe, H.; Sasaki, Y.; Katagiri, H.; Wang, X.-F.; Sano, T.; Hong, Z.; Yang, Y.; Kido, J. A Series of Squaraine Dyes: Effects of Side Chain and the Number of Hydroxyl Groups on Material Properties and Photovoltaic Performance. *Chem. Mater.* **2014**, *26*, 1356−1364.

(8) Corredor, C. C.; Huang, Z.-L.; Belfield, K. D. Two-Photon 3D Optical Data Storage via Fluorescence Modulation of an Efficient Fluorene Dye by a Photochromic Diarylethene. *Adv. Mater.* **2006**, *18*, 2910−2914.

(9) Emmelius, M.; Pawlowski, G.; Vollmann, H. W. Materials for Optical Data Storage. *Angew. Chem., Int. Ed.* **1989**, *28*, 1445−1471.

(10) Jipson, V. B.; Jones, C. R. Infrared dyes for optical storage. *J. Vac. Sci. Technol.* **1981**, *18*, 105−109.

(11) Karpenko, I. A.; Klymchenko, A. S.; Gioria, S.; Kreder, R.; Shulov, I.; Villa, P.; Mély, Y.; Hibert, M.; Bonnet, D. Squaraine as a Bright, Stable and Environment-Sensitive Far-Red Label for Receptor-Specific Cellular Imaging. *Chem. Commun.* **2015**, *51*, 2960−2963.

(12) Luo, C.; Zhou, Q.; Jiang, G.; He, L.; Zhang, B.; Wang, X. The synthesis and $^1O_2$ photosensitization of halogenated asymmetric aniline-based squaraines. *New J. Chem.* **2011**, *35*, 1128−1132.

(13) Kurhuzenkau, S. A.; Woodward, A. W.; Yao, S.; Belfield, K. D.; Shaydyuk, Y. O.; Sissa, C.; Bondar, M. V.; Painelli, A. Ultrafast Spectroscopy, Superluminescence and Theoretical Modeling of a Two-Photon Absorbing Fluorene Derivative. *Phys. Chem. Chem. Phys.* **2016**, *18*, 12839−12846.

(14) Zhang, Y.; Kim, B.; Yao, S.; Bondar, M. V.; Belfield, K. D. Controlled Aggregation and Enhanced Two-Photon Absorption of a Water-Soluble Squaraine Dye with a Poly(acrylic acid) Template. *Langmuir* **2013**, *29*, 11005−11012.

(15) Sun, C.-L.; Liao, Q.; Li, T.; Li, J.; Jiang, J.-Q.; Xu, Z.-Z.; Wang, X.-D.; Shen, R.; Bai, D.-C.; Wang, Q.; Zhang, S.-X.; Fu, H.-B.; Zhang, H.-L. Rational Design of Small Indolic Squaraine Dyes with Large Two-Photon Absorption Cross Section. *Chem. Sci.* **2015**, *6*, 761−769.

(16) Zhang, G.; Zhao, J.; Chow, P. C. Y.; Jiang, K.; Zhang, J.; Zhu, Z.; Zhang, J.; Huang, F.; Yan, H. Nonfullerene Acceptor Molecules for Bulk Heterojunction Organic Solar Cells. *Chem. Rev.* **2018**, *118*, 3447−3507.

(17) Nielsen, C. B.; Holliday, S.; Chen, H.-Y.; Cryer, S. J.; McCulloch, I. Non-Fullerene Electron Acceptors for Use in Organic Solar Cells. *Acc. Chem. Res.* **2015**, *48*, 2803−2812.

(18) Yan, C.; Barlow, S.; Wang, Z.; Yan, H.; Jen, A. K.-Y.; Marder, S. R.; Zhan, X. Non-fullerene Acceptors for Organic Solar Cells. *Nat. Rev. Mater.* **2018**, *3*, 18003.

DOI: 10.1021/acsomega.8b01809
ACS Omega 2018, 3, 15416−15425

(19) Cheng, P.; Li, G.; Zhan, X.; Yang, Y. Next-generation Organic Photovoltaics based on Non-fullerene Acceptors. *Nat. Photonics* **2018**, *12*, 131−142.
(20) Wang, K.; Firdaus, Y.; Babics, M.; Cruciani, F.; Saleem, Q.; El Labban, A.; Alamoudi, M. A.; Marszalek, T.; Pisula, W.; Laquai, F.; Beaujuge, P. M. π-Bridge-Independent 2-(Benzo[c][1,2,5]thiadiazol-4-ylmethylene)malononitrile-Substituted Nonfullerene Acceptors for Efficient Bulk Heterojunction Solar Cells. *Chem. Mater.* **2016**, *28*, 2200−2208.
(21) Kim, Y.; Song, C. E.; Moon, S.-J.; Lim, E. Rhodanine dye-based small molecule acceptors for organic photovoltaic cells. *Chem. Commun.* **2014**, *50*, 8235−8238.
(22) Wu, Y.; Bai, H.; Wang, Z.; Cheng, P.; Zhu, S.; Wang, Y.; Ma, W.; Zhan, X. A Planar Electron Acceptor for Efficient Polymer Solar Cells. *Energy Environ. Sci.* **2015**, *8*, 3215−3221.
(23) Bai, H.; Wu, Y.; Wang, Y.; Wu, Y.; Li, R.; Cheng, P.; Zhang, M.; Wang, J.; Ma, W.; Zhan, X. Nonfullerene acceptors based on extended fused rings flanked with benzothiadiazolylmethylenemalononitrile for polymer solar cells. *J. Mater. Chem. A* **2015**, *3*, 20758−20766.
(24) Lv, A.; Stolte, M.; Würthner, F. Head-to-Tail Zig-Zag Packing of Dipolar Merocyanine Dyes Affords High-Performance Organic Thin-Film Transistors. *Angew. Chem., Int. Ed.* **2015**, *54*, 10512−10515.
(25) Liess, A.; Huang, L.; Arjona-Esteban, A.; Lv, A.; Gsänger, M.; Stepanenko, V.; Stolte, M.; Würthner, F. Organic Thin Film Transistors Based on Highly Dipolar Donor-Acceptor Polymethine Dyes. *Adv. Funct. Mater.* **2015**, *25*, 44−57.
(26) Heiniger, L.-P.; O'Brien, P. G.; Soheilnia, N.; Yang, Y.; Kherani, N. P.; Grätzel, M.; Ozin, G. A.; Tétreault, N. See-Through Dye-Sensitized Solar Cells: Photonic Reflectors for Tandem and Building Integrated Photovoltaics. *Adv. Mater.* **2013**, *25*, 5734−5741.
(27) Tai, Q.; Yan, F. Emerging Semitransparent Solar Cells: Materials and Device Design. *Adv. Mater.* **2017**, *29*, 1700192.
(28) Keil, D.; Hartmann, H.; Moschny, T. Synthesis and characterization of 1,3-bis-(2-dialkylamino-5-thienyl)-substituted squaraines—a novel class of intensively coloured panchromatic dyes. *Dyes Pigm.* **1991**, *17*, 19−27.
(29) Sreejith, S.; Carol, P.; Chithra, P.; Ajayaghosh, A. Squaraine Dyes: A Mine of Molecular Materials. *J. Mater. Chem.* **2008**, *18*, 264−274.
(30) Mayerhöffer, U.; Deing, K.; Gruß, K.; Braunschweig, H.; Meerholz, K.; Würthner, F. Outstanding Short-Circuit Currents in BHJ Solar Cells Based on NIR-Absorbing Acceptor-Substituted Squaraines. *Angew. Chem., Int. Ed.* **2009**, *48*, 8776−8779.
(31) Wang, S.; Hall, L.; Diev, V. V.; Haiges, R.; Wei, G.; Xiao, X.; Djurovich, P. I.; Forrest, S. R.; Thompson, M. E. N,N-Diarylanilinosquaraines and Their Application to Organic Photovoltaics. *Chem. Mater.* **2011**, *23*, 4789−4798.
(32) Sun, Y.; Welch, G. C.; Leong, W. L.; Takacs, C. J.; Bazan, G. C.; Heeger, A. J. Solution-Processed Small-Molecule Solar Cells with 6.7% Efficiency. *Nat. Mater.* **2012**, *11*, 44−48.
(33) McDowell, C.; Narayanaswamy, K.; Yadagiri, B.; Gayathri, T.; Seifrid, M.; Datt, R.; Ryno, S. M.; Heifner, M. C.; Gupta, V.; Risko, C.; Singh, S. P.; Bazan, G. C. Impact of Rotamer Diversity on the Self-Assembly of Nearly Isostructural Molecular Semiconductors. *J. Mater. Chem. A* **2018**, *6*, 383−394.
(34) Rao, G. H.; Rana, P. J. S.; Islam, A.; Singh, S. P. Synthesis of Multichromophoric Asymmetrical Squaraine Sensitizer via C-H Arylation for See-through Photovoltaic. *ACS Appl. Energy Mater.* **2018**, *1*, 4786−4793.
(35) Marchena, M. J.; de Miguel, G.; Cohen, B.; Organero, J. A.; Pandey, S.; Hayase, S.; Douhal, A. Real-Time Photodynamics of Squaraine-Based Dye-Sensitized Solar Cells with Iodide and Cobalt Electrolytes. *J. Phys. Chem. C* **2013**, *117*, 11906−11919.
(36) Sung, J.; Kim, P.; Lee, Y. O.; Kim, J. S.; Kim, D. Characterization of Ultrafast Intramolecular Charge Transfer Dynamics in Pyrenyl Derivatives: Systematic Change of the Number of Peripheral N,N-Dimethyaniline Substituents. *J. Phys. Chem. Lett.* **2011**, *2*, 818−823.
(37) Zhang, G.; Musgrave, C. B. Comparison of DFT Methods for Molecular Orbital Eigenvalue Calculations. *J. Phys. Chem. A* **2007**, *111*, 1554−1561.
(38) Prabhakar, C.; Chaitanya, G. K.; Sitha, S.; Bhanuprakash, K.; Rao, V. J. Role of the Oxyallyl Substructure in the Near Infrared (NIR) Absorption in Symmetrical Dye Derivatives: A Computational Study. *J. Phys. Chem. A* **2005**, *109*, 2614−2622.
(39) Prabhakar, C.; Yesudas, K.; Krishna Chaitanya, G.; Sitha, S.; Bhanuprakash, K.; Rao, V. J. Near-Infrared Absorption in Symmetric Squarylium and Croconate Dyes: A Comparative Study Using Symmetry-Adapted Cluster-Configuration Interaction Methods. *J. Phys. Chem. A* **2005**, *109*, 8604−8616.
(40) Yamanaka, S.; Okumura, M.; Nakano, M.; Yamaguchi, K. EHF theory of chemical reactions Part 4. UNO CASSCF, UNO CASPT2 and R(U)HF coupled-cluster (CC) wavefunctions. *J. Mol. Struct.* **1994**, *310*, 205−218.
(41) Nakano, M.; et al. Second Hyperpolarizabilities (γ) of Bisimidazole and Bistriazole Benzenes: Diradical Character, Charged State, and Spin State Dependences. *J. Phys. Chem. A* **2006**, *110*, 4238−4243.
(42) Nakano, M.; et al. Origin of the Enhancement of the Second Hyperpolarizability of Singlet Diradical Systems with Intermediate Diradical Character. *J. Chem. Phys.* **2006**, *125*, 074113.
(43) Völker, S. F.; Renz, M.; Kaupp, M.; Lambert, C. Squaraine Dyes as Efficient Coupling Bridges between Triarylamine Redox Centres. *Chem.—Eur. J.* **2011**, *17*, 14147−14163.
(44) Mao, J.; He, N.; Ning, Z.; Zhang, Q.; Guo, F.; Chen, L.; Wu, W.; Hua, J.; Tian, H. Stable Dyes Containing Double Acceptors without COOH as Anchors for Highly Efficient Dye-Sensitized Solar Cells. *Angew. Chem.* **2012**, *124*, 10011−10014.
(45) Frisch, M. J.; Trucks, G. W.; Schlegel, H. B.; Scuseria, G. E.; Robb, M. A.; Cheeseman, J. R.; Scalmani, G.; Barone, V.; Mennucci, B.; Petersson, G. A.;et al. *Gaussian 09*, Revision D.01; Gaussian, Inc.: Wallingford, CT, 2013.
(46) Becke, A. D. Density-functional thermochemistry. III. The role of exact exchange. *J. Chem. Phys.* **1993**, *98*, 5648−5652.
(47) Thomas, A.; Srinivas, K.; Prabhakar, C.; Bhanuprakash, K.; Rao, V. J. Estimation of the First Excitation Energy in Diradicaloid Croconate Dyes Having Absorption in the near Infra Red (NIR): A DFT and SF-TDDFT Study. *Chem. Phys. Lett.* **2008**, *454*, 36−41.
(48) Chitumalla, R. K.; Lim, M.; Gao, X.; Jang, J. Substituent Effects on the Croconate Dyes in Dye Sensitized Solar Cell Applications: A Density Functional Theory Study. *J. Mol. Model.* **2015**, *21*, 297.
(49) Miertuš, S.; Scrocco, E.; Tomasi, J. Electrostatic Interaction of a Solute with a Continuum. A Direct Utilizaion of AB Initio Molecular Potentials for the Prevision of Solvent Effects. *Chem. Phys.* **1981**, *55*, 117−129.
(50) Cossi, M.; Barone, V.; Cammi, R.; Tomasi, J. Ab initio study of solvated molecules: a new implementation of the polarizable continuum model. *Chem. Phys. Lett.* **1996**, *255*, 327−335.
(51) Dennington, R.; Keith, T.; Millam, J. *GaussView*, version 5; Semichem Inc.: Shawnee Mission, KS, 2009.

DOI: 10.1021/acsomega.8b01809
ACS Omega 2018, 3, 15416−15425